THE
EMBO
JOURNAL

The nuclear receptor PPARγ individually responds to serotonin- and fatty acid-metabolites

Tsuyoshi Waku[1,3], Takuma Shiraki[2,3], Takuji Oyama[1], Kanako Maebara[1], Rinna Nakamori[1] and Kosuke Morikawa[1,*]

[1]The Takara Bio Endowed Division, Department of Biomolecular Recognition, Institute for Protein Research, Osaka University, Open Laboratories of Advanced Bioscience and Biotechnology, Furuedai, Suita, Osaka, Japan and [2]Department of Biochemistry, Tohoku University Graduate School of Medicine, Aoba-ku, Sendai, Miyagi, Japan

The nuclear receptor, peroxisome proliferator-activated receptor γ (PPARγ), recognizes various synthetic and endogenous ligands by the ligand-binding domain. Fatty-acid metabolites reportedly activate PPARγ through conformational changes of the Ω loop. Here, we report that serotonin metabolites act as endogenous agonists for PPARγ to regulate macrophage function and adipogenesis by directly binding to helix H12. A cyclooxygenase inhibitor, indomethacin, is a mimetic agonist of these metabolites. Crystallographic analyses revealed that an indole acetate functions as a common moiety for the recognition by the sub-pocket near helix H12. Intriguingly, a serotonin metabolite and a fatty-acid metabolite each bind to distinct sub-pockets, and the PPARγ antagonist, T0070907, blocked the fatty-acid agonism, but not that of the serotonin metabolites. Mutational analyses on receptor-mediated transcription and coactivator binding revealed that each metabolite individually uses coregulator and/or heterodimer interfaces in a ligand-type-specific manner. Furthermore, the inhibition of the serotonin metabolism reduced the expression of the endogenous PPARγ-target gene. Collectively, these results suggest a novel agonism, in which PPARγ functions as a multiple sensor in response to distinct metabolites.

Introduction

The nuclear receptor, peroxisome proliferator-activated receptor γ (PPARγ), is a ligand-dependent transcription factor that coordinates gene expression related to glucose homeostasis and insulin sensitization (Evans *et al*, 2004; Lehrke and Lazar, 2005; McKenna *et al*, 2009). In contrast to the adipocyte-specific expression of the PPARγ2 isoform, macrophage cells express the PPARγ1 isoform, which has crucial functions in lipid metabolism and inflammatory function, such as cytokine production (Ricote *et al*, 1998; Huang *et al*, 1999). The macrophage-specific deletion of the *Pparg* gene in mice causes diet-induced obesity and insulin resistance, indicating that this receptor regulates glucose and lipid homeostasis and tissue inflammation (Odegaard *et al*, 2007).

PPARγ is thus a potential therapeutic target for metabolic syndrome and inflammatory diseases (i.e. type II diabetes and atherosclerosis) (Walczak and Tontonoz, 2002; Waki *et al*, 2007). A well-known class of synthetic PPARγ agonists, thiazolidine derivatives (TZDs), is used for anti-diabetic and anti-inflammatory therapies (Ceriello, 2008). Another class of agonists has recently been developed to reduce the side effects of TZDs, such as weight gain and heart-attack risk (Berger *et al*, 2005). These synthetic agonists are categorized as 'full' and 'partial' agonists, depending on their transcriptional activities in the cell-based reporter assay (Reginato *et al*, 1998).

To rationally design drugs for PPARγ, substantial efforts have been made to understand the structure–function relationships of the receptor activation by each agonist. The direct interaction between a ligand and the C-terminal helix in the ligand-binding domain (LBD), constituting the activation function 2 (AF-2), reportedly has a crucial function in the ligand-induced receptor activation by forming binding interfaces with members of the steroid receptor coactivator (SRC) family, especially with its LXXLL motif (where X denotes any amino acid) (Li *et al*, 2003; Nagy and Schwabe, 2004). In fact, full agonists, such as BRL49653, form a hydrogen bond with Tyr473 on the AF-2 helix H12 (Nolte *et al*, 1998), whereas partial agonists, such as GW0072, do not always interact with this helix to activate PPARγ (Oberfield *et al*, 1999) (Figure 1A–C). The formation of this hydrogen bond with helix H12 is also considered to cause the difference between the full and partial activities, thus leading to the conclusion that the direct interaction with helix H12 has a central function in regulating the ligand-induced PPARγ activities.

On the other hand, several polyunsaturated fatty-acid metabolites, produced through cyclooxygenase (COX)- or lipoxygenase-mediated pathways, function as potent endogenous ligands for this receptor in adipocyes and macrophages (Forman *et al*, 1995; Kliewer *et al*, 1995; Huang *et al*, 1999; Schopfer *et al*, 2005; Shiraki *et al*, 2005a). Our recent studies revealed that several oxidized fatty-acid metabolites, including 15-oxo-eicosatetraenoic acid (15-oxoETE), do not always require the interaction with helix H12 for receptor activation (Waku *et al*, 2009a). Indeed, the type of endogenous ligand that binds to the sub-pocket adjacent to helix H12 (Figure 1C, enclosed area) is still unknown, and thus PPARγ is as a crucial target for structural studies to clarify the controversial issue of the ligand-dependent activation mechanism, which is referred to as 'agonism'.

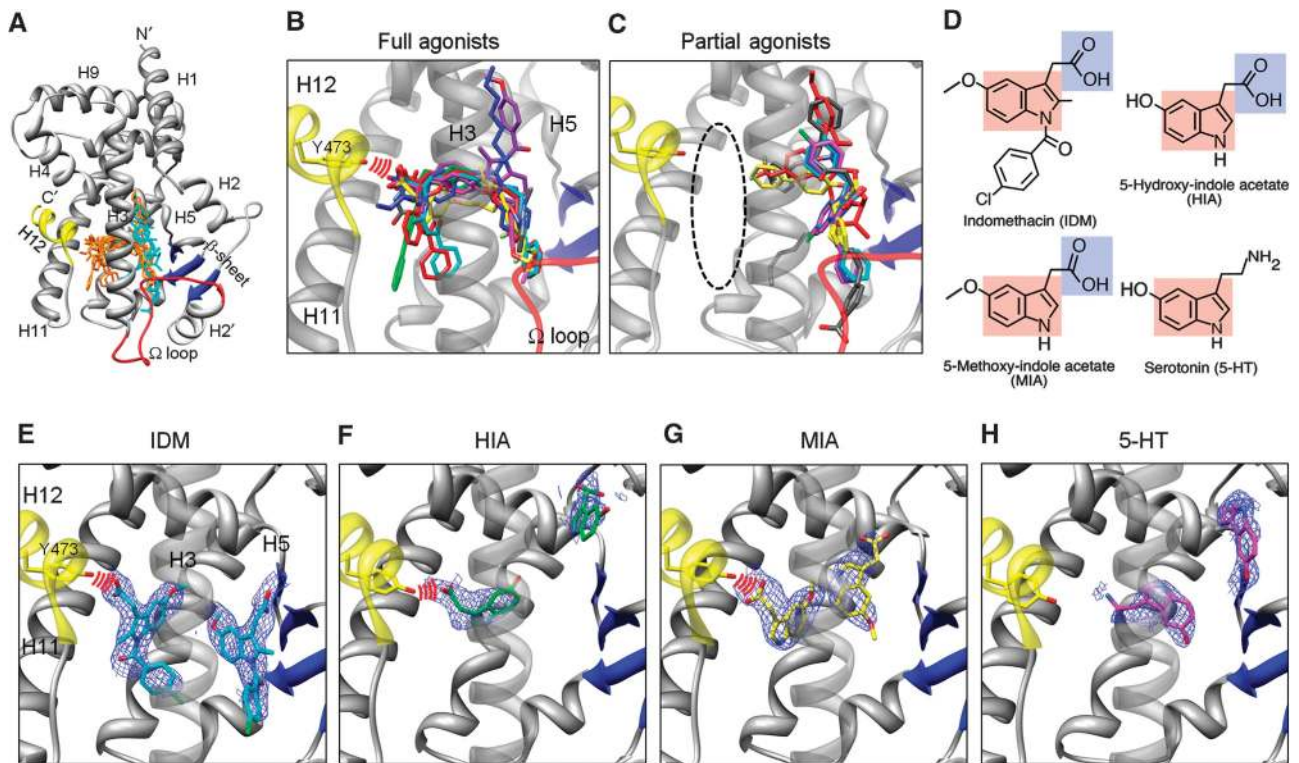*Corresponding author. The Takara-Bio Endowed Division, Department of Biomolecular Recognition, Institute for Protein Research, Osaka University, 6-2-3 Furuedai, Suita, Osaka 565-0874, Japan.
Tel.: +81 66 872 8200; Fax: +81 66 872 8219;
E-mail: morikako@protein.osaka-u.ac.jp
[3]These authors contributed equally to this work

Figure 1 Configurations of indole acetate-containing ligands and known agonists in the PPARγ LBD. (**A**) Superposition of known agonists in PPARγ LBDs. Full agonists (orange) and partial ones (cyan) are shown within the apo-LBD (2ZK0; Waku *et al*, 2009a). The Cα atoms of the LBD are coloured yellow (helix H12), red (Ω loop), blue (β-sheet), and grey (other region). Full agonists are from PDB 2PRG (Nolte *et al*, 1998); 1FM9 (Gampe *et al*, 2000); 1I7I (Cronet *et al*, 2001); 1K74 (Xu *et al*, 2001); 2ATH (Mahindroo *et al*, 2005); 2I4J (Pochetti *et al*, 2007); 2Q59 (Bruning *et al*, 2007); and 3B3K (Montanari *et al*, 2008). Partial agonists are from 4PRG: Oberfield *et al*, 1999); 2Q5P, 2Q5S, 2Q6R, and 2Q61(Bruning *et al*, 2007); and 3D6D (Montanari *et al*, 2008). (**B**) Close-up view of the full agoinsts. Red arcs indicate hydrogen bonds between full agonists and Tyr473. (**C**) Close-up view of the partial agonists. The area enclosed by the black dashed line is the AF-2 pocket. (**D**) Chemical structures of IDM, 5-HT, HIA, and MIA. The indole ring and the carboxyl group are coloured red and blue, respectively. (**E–H**) Crystal structures of the PPARγ LBDs in complex with indole acetate-containing ligands. IDM is coloured cyan (**E**), HIA is green (**F**), MIA is yellow (**G**), and 5-HT is magenta (**H**), in close-up views with the omit 2Fo-Fc map (contoured at 1σ). The LBD and the hydrogen bonds between each molecule and Tyr473 are represented as described in (**A**) and (**B**).

Serotonin (5-HT) is an extracellular signalling molecule that activates its specific receptors on the plasma membrane. Extracellular 5-HT is subsequently incorporated into the surrounding cells by its specific transporter SERT and is metabolized into 5-methoxy-indole acetate (MIA) through 5-hydroxy-indole acetate (HIA) by several enzymes, including monoamine oxidase (MAO) (Supplementary Figure S1A). In addition to the receptor-mediated action, 5-HT also coordinates fat metabolism and feeding through a receptor-independent mechanism (Srinivasan *et al*, 2008). Other reports described the association between *MAO* expression and insulin sensitization (Fontana *et al*, 2001) and that between MAO polymorphism and obesity (Fuemmeler *et al*, 2008). These reports suggested that 5-HT metabolites are not simply degradation products of 5-HT, but may have additional functions. A COX inhibitor, indomethacin (IDM), directly activates PPARγ (Lehmann *et al*, 1997). Notably, this synthetic compound has an indole acetate, which is commonly found in several 5-HT metabolites. These findings tempted us to investigate the possibility of their common mechanism in PPARγ activation.

Here, we performed X-ray crystallographic and biochemical analyses, and revealed that IDM, HIA, and MIA, which in common contain an indole acetate, bind to the sub-pocket by directly interacting with Tyr473 of the PPARγ LBD. These indole acetate-containing ligands activated this receptor, which is

endogenously expressed within macrophage-like cells and adipogenic fibroblasts. Intriguingly, an indole acetate-containing ligand and a fatty acid simultaneously occupy distinct sub-pockets, which are located adjacent to the AF-2 and the Ω loop. The covalent modification of Cys285 by the antagonist, T0070907, inhibited the activation of PPARγ by a TZD agonist or a fatty-acid ligand, whereas it did not affect the activation by an indole acetate-containing ligand. Mutational analyses suggested that ligand binding to each sub-pocket induces structural alterations of different sites on the outer LBD surfaces, which interact with the coregulator and the heterodimer partner, indicating that the sub-pockets near the AF-2 helix H12 and the Ω loop (hereafter referred to as the AF-2 and the Ω pockets, respectively) are individually specialized for the recognition of 5-HT- and fatty acid-metabolites. We further revealed that the 5-HT-induced expression of the PPARγ-target gene was inhibited by blocking the endogenous SERT or MAO. Therefore, these results suggest that PPARγ may individually respond to the two-independent metabolic pathways.

Results

Indole acetate-containing ligands directly interact with helix H12

Initially, we searched for the particular chemical moiety of the ligands specifically recognized by the AF-2 pocket

(Figure 1C, enclosed area). A Protein Data Bank (PDB) search revealed that 5-methoxy-indole propionate binds to this sub-pocket (Artis *et al*, 2009). As the COX inhibitor IDM, containing an indole acetate, also activates PPARγ (Lehmann *et al*, 1997), we hypothesized that an indole ring connected to a carboxyl group may function as the core moieties for binding to the AF-2 pocket. Among the endogenous metabolites, two 5-HT metabolites, HIA and MIA, contain both the indole ring and carboxyl group moieties, whereas 5-HT itself contains an indole ring, but lacks the carboxyl group (Figure 1D). To examine whether these metabolites can bind to PPARγ LBD, we performed a surface plasmon resonance (SPR) analysis. The PPARγ LBD protein was captured on the sensor chip, on which each ligand was applied in a series of five concentrations (Supplementary Figure S1B–E). From the SPR signals, the dissociation constants (K_d) of IDM, HIA, MIA, and 5-HT were calculated as 9.73, 28.0, 72.8, and 933 µM, respectively.

We then investigated whether these synthetic and endogenous molecules occupy the AF-2 pocket by X-ray crystallography (see Materials and methods for the description of the structural figures; Supplementary Figures S2A–D; Table S1). The atomic structure of the LBD in complex with each ligand revealed that IDM, HIA, and MIA directly interact with Tyr473 on helix H12 through a hydrogen bond, although 5-HT, located in the middle between the two sub-pockets, does not contact this helix (Figure 1E–H; Supplementary Figure S3). Unexpectedly, another molecule of each ligand binds to the Ω pocket. Structural comparisons among the complexes revealed that the configurations of IDM, HIA, and MIA are similar in the AF-2 pocket, whereas they differed in the Ω pocket (Supplementary Figure S4). Furthermore, the refinement statistics of these crystal structures of the ligand/PPARγ LBD complexes, produced at a molar ratio of 1:5 (0.1 mM ligand: approximately 0.5 mM protein), revealed that the average *B*-factors of IDM and MIA in the AF-2 pocket are lower than those in the Ω pocket (Supplementary Figure S4B and C). For example, the average *B*-factors of IDM molecules in the AF-2 and Ω pockets are 80.33 and 106.8 Å², respectively. The IDM/PPARγ LBD complex, produced at a molar ratio of 10:1 (5 mM ligand: approximately 0.5 mM protein), exhibited the corresponding values of 56.76 and 81.10 Å², respectively (data not shown), thus suggesting that the indole acetate, with both the indole ring and carboxyl group, serves as the core moiety to preferentially bind to the AF-2 pocket. We hereafter refer to IDM, MIA, and HIA as the indole acetate-containing ligands.

Indole acetate-containing ligands are AF-2-dependent agonists

To examine whether the indole acetate-containing ligands actually activate PPARγ, we performed a cell-based reporter assay using HEK293T cells and Gal4 DNA-binding domain (DBD)-fused PPARγ LBD (Gal4DBD-PPARγLBD). MIA and IDM, which each directly interact with helix H12, activated PPARγ, whereas 5-HT, which lacks contact with this helix, did not induce the receptor activation (Figure 2A). Although HIA is an indole acetate-containing ligand (see above), this ligand did not activate PPARγ (Figure 2A). As the HEK293T cells were maintained in culture medium containing a large amount (over 70 µM) of L-tryptophan, the precursor of 5-HT, the 5-HT metabolic status in these cells may cause the

unexpected alteration of the responsiveness to its metabolites, HIA and MIA (Supplementary Figure S1A).

To explore the physiological aspects of 5-HT metabolites in regulating PPARγ activity, we further investigated each agonistic function of the indole acetate-containing ligands in phorbol 12-myristate 13-acetate (PMA)-activated THP-1 cells. This macrophage-like cell endogenously expresses PPARγ, and its cellular function is regulated by the activity of this receptor (Ricote *et al*, 1998; Huang *et al*, 1999; Odegaard *et al*, 2007). In this cell line, IDM, HIA, and MIA up-regulated two PPARγ-target genes, acyl-CoA oxidase (*AOX*) and liver X receptor α (*LXRα*), similarly to BRL49653 (Marcus *et al*, 1993; Laffitte *et al*, 2001) (Figure 2B). We also validated their activities for the adipogenic differentiation of 3T3-L1 cells, which is strongly dependent on PPARγ (Forman *et al*, 1995). Oil red O staining of lipid accumulation within the cells revealed that the PPARγ ligand, 15-deoxy-$\Delta^{12,14}$-prostaglandin J$_2$ (15d-PGJ$_2$), promoted adipogenesis in the cells (Figure 2C). IDM and MIA also induced a similar effect (Figure 2C), indicating that the indole acetate-containing ligands act as PPARγ agonists.

To clarify whether the indole acetate-containing ligands function through the AF-2 pocket, we replaced Tyr473 on the helix H12 by phenylalanine (Y473F) and examined the influence of the mutation on the binding of the indole acetate-containing ligands within the AF-2 pocket. This mutation did not cause any alterations in the expression and the stability of the Gal4DBD-PPARγLBD protein in the cells (Figure 2D), suggesting that the structural integrity of the receptor is unchanged. However, this mutant PPARγ was totally insensitive to IDM or MIA (Figure 2E), indicating that the indole acetate ligands activate PPARγ through the AF-2 pocket. To clarify the effect of the mutation on the ligand-binding mode, we determined the K_d values for IDM by isothermal titration calorimetry (ITC). The WT-LBD showed two K_d values for IDM ($K_d1 = 17.24$ µM and $K_d2 = 934.5$ µM) (Figure 2F, left panel). In contrast, the Y473F mutant showed reduced affinity, with only one K_d value for IDM ($K_d = 980.0$ µM) (Figure 2F, right panel). The disappearance of K_d1 in the Y473F mutant is consistent with the notion that the indole acetate-containing ligands preferentially bind to the AF-2 pocket to activate the receptor.

Crystal structures of PPARγ LBD complexes containing two distinct ligands

Two recent papers reported that PPARγ recognizes a fatty-acid ligand, such as 15-oxoETE and 9-(*S*)-hydroxyoctadecadienoic acid, by the Ω pocket (Itoh *et al*, 2008; Waku *et al*, 2009a). Thus, we presumed that fatty acid and indole acetate-containing ligands could simultaneously bind to the Ω and AF-2 pockets, respectively.

To address this hypothesis, we determined two crystal structures of LBD complexes, with the indole acetate-containing ligand and the fatty-acid ligand (Supplementary Figure S2E and F; Table S1): one crystal was prepared with a pair of metabolite ligands, MIA and 15-oxoETE, and the other with the corresponding synthetic ligands, IDM and nitro-233, the latter of which was identified as a mimetic agonist of 15-oxoETE (Waku *et al*, 2009a). Each indole acetate-containing ligand, MIA and IDM, occupied the AF-2 pocket, and directly interacted with Tyr473 on helix H12. In contrast, the fatty-acid ligands, 15-oxoETE and nitro-233, each bound
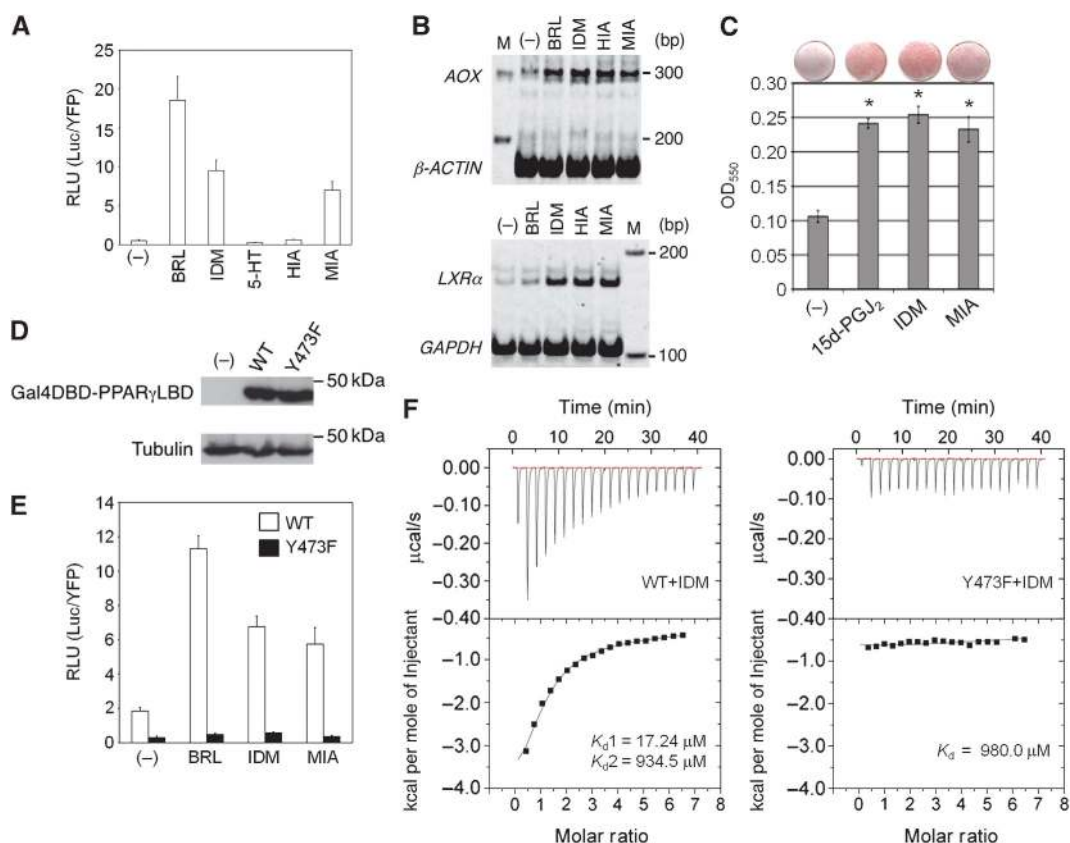
Figure 2 Characterization of indole acetate-containing ligands as AF-2-mediated agonists for PPARγ. (**A**) Effects of each indole acetate-containing ligand on the activity of the Gal4DBD-PPARγLBD. The final concentrations of BRL49653 (BRL) and IDM were 1 and 10 μM, respectively. The concentrations of 5-HT, HIA, and MIA were 100 μM. The RLU (Luc/YFP) is shown with + s.d. ($n = 4$). (**B**) Effects on the ligand-induced expression of the endogenous PPARγ-target genes *AOX* and *LXRα* in PMA-activated macrophage-like THP-1 cells. After activation by PMA, the cells were treated with 1 μM BLR49653 (BRL), 10 μM IDM, 100 μM HIA, and 100 μM MIA, respectively. *β-ACTIN* and *GAPDH* were used as references. (**C**) Effects on 3T3-L1 adipogenesis. After a pre-treatment with 1 μM Dex, 0.5 mM IBMX, and 5 μg/ml insulin, the cells were incubated with 10 μM 15d-PGJ₂, 10 μM IDM, or 100 μM MIA, respectively. Oil red O stained cells are shown at the top and are quantified at the bottom by measurement at the OD₅₅₀ with ± s.d. The statistical comparison of each ligand with a negative control (DMSO) was accomplished using the Mann–Whitney *U*-test. *$P < 0.05$. $n = 4$. (**D**) Effect of the Y473F mutation on the protein stability of Gal4DBD-PPARγLBD. The wild type (WT) and the Y473F mutant were transfected into HEK293T cells. After 1 day, the cells were collected and analysed by immunoblotting with an anti-Gal4 DBD antibody. Mock-transfected cells (-) were used as a negative control, and tubulin was used as a reference. (**E**) Effects of the Y473F mutation on the ligand-induced activity of Gal4DBD-PPARγLBD. Open and closed bars show the ligand-induced activities of the wild type (WT) and the mutant (Y473F), respectively. BRL49653 (BRL), IDM, and MIA were added at final concentrations of 1, 10, and 100 μM, respectively. The RLU (Luc/YFP) is shown with + s.d. ($n = 4$). (**F**) Effects of the Y473F mutation on the IDM binding to the PPARγ LBD. The direct interactions of IDM with the wild type (WT) and the Y473F mutant PPARγ LBD were quantitatively analysed by ITC, as shown in the left and right panels, respectively.

to the Ω pocket (Figure 3A; Supplementary Figure S5). Furthermore, the electron densities clearly indicated the formation of a covalent bond between the α,β-unsaturated ketone of 15-oxoETE (or the α,β-unsaturated nitro of nitro-233) and the sulfhydryl group of Cys285 through a Michael addition (Figure 3A; Supplementary Figure S5, insets), in agreement with our previous results (Waku *et al*, 2009a).

Two distinct ligands simultaneously bind different sub-pockets in solution

To confirm whether two distinct ligands simultaneously bind to the LBD in solution, we developed a novel ligand-binding assay based on fluorescent resonance energy transfer (FRET). As 15-oxoETE lacks intrinsic fluorescence, we used the fluorescent fatty-acid analogue C8-BODIPY (Figure 3B). This fatty-acid analogue did not activate PPARγ (data not shown), but non-covalently bound to PPARγ in a similar ligand configuration to 15-oxoETE in the crystal structure

(Supplementary Figures 3C and S2G; Table S1). In the native PAGE gel, the protein band corresponding to the PPARγ LBD exhibited the fluorescence in the presence of C8-BODIPY, and this fluorescence disappeared upon the addition of 15-oxoETE in a dose-dependent manner (Figure 3D, left panel). In contrast, the fluorescence was not affected by the addition of IDM or MIA (Figure 3D, middle and right panels, respectively), suggesting that C8-BODIPY did not compete with either IDM or MIA. C8-BODIPY, with a major excitation wavelength at 480 nm, also has a secondary excitation wavelength at 355 nm, which corresponds to the emission wavelength of the indole ring in MIA. Accordingly, FRET should only occur between MIA and C8-BODIPY when they are simultaneously accommodated within the LBD (Figure 3E). The LBD lacks a fluorescent tryptophan, and thus FRET should exclusively provide information about simultaneous ligand binding. Using this assay, we observed that the binding of MIA to the LBD did not change the
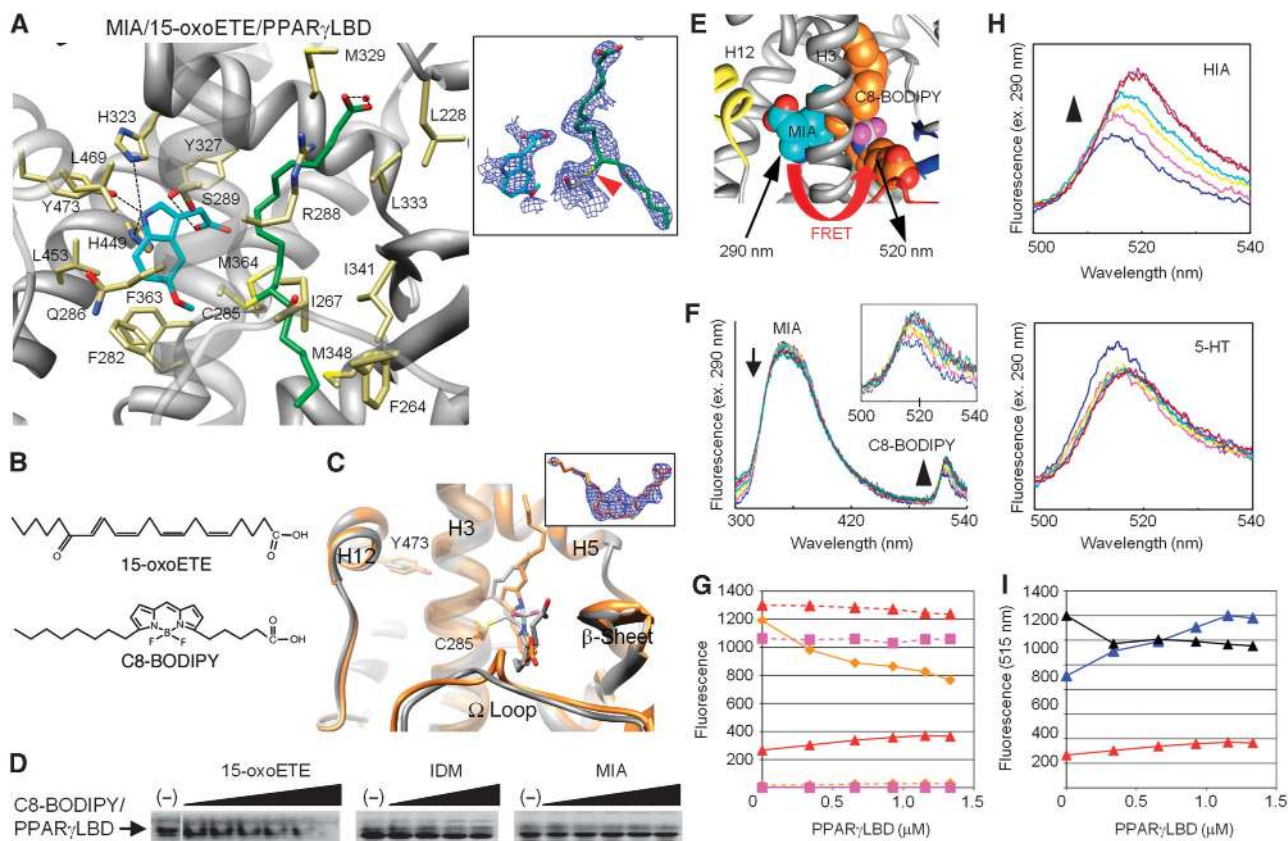
Figure 3 Crystallographic and biochemical analyses of simultaneous ligand binding. (**A**) Crystal structure of the PPARγ LBD with two metabolites, MIA (cyan) and 15-oxoETE (green). The side chains that interact with ligands are shown (light yellow). A red sphere represents a water molecule. Black dashed lines indicate hydrogen bonds between the ligand and the side chains or the water molecule. In the inset, the omit 2Fo-Fc map is shown (contoured at 1σ) with a red arrowhead, indicating the covalent bond between 15-oxoETE and Cys285. (**B**) Chemical structures of 15-oxoETE and C8-BODIPY. (**C**) Structural alignment of C8-BODIPY (orange) and 15-oxoETE (PDB 2ZK5 in grey: Waku et al, 2009a) in the PPARγ LBD complex. The inset displays the omit 2Fo-Fc map of C8-BODIPY (contoured at 1σ). (**D**) Ligand-binding assay using native PAGE. 15-oxoETE was added simultaneously with 0.1 μM C8-BODIPY, at concentrations of 0.001, 0.01, 0.1, 1.0, 10, and 30 μM. Similarly, IDM was added at concentrations of 0.1, 1.0, 10, and 100 μM, and MIA was added at concentrations of 0.1, 1.0, 10, 100, and 300 μM. (**E**) Structural representation of the simultaneous ligand-binding assay, based on FRET. This model was made by superimposing the MIA in the AF-2 pocket onto the C8-BODIPY/LBD structure. (**F**) LBD-dependent change of FRET spectra between C8-BODIPY and MIA. The LBD protein was added to the mixture of C8-BODIPY with MIA, at final concentrations of 0 (blue line), 0.34 (magenta), 0.66 (yellow), 0.93 (cyan), 1.16 (dark purple), 1.34 (brown), and 1.47 μM (dark green). The arrow indicates the FRET-dependent decrease of the MIA fluorescence, and the inset shows a close-up view of the FRET-dependent increase of C8-BODIPY fluorescence, ranging from 500 nm to 540 nm. (**G**) Plot of MIA and C8-BODIPY fluorescence in response to the addition of the LBD protein. Symbols represent the 355 nm fluorescence of MIA in the presence of C8-BODIPY (dashed line with triangles), the 515 nm fluorescence of C8-BODIPY in the presence of MIA (solid line with triangles), MIA alone (square with magenta dashed line at 355 nm or solid line at 515 nm) and C8-BODIPY alone (diamonds with orange dashed line at 355 nm or solid line at 515 nm). (**H**) FRET-dependent spectral changes of C8-BODIPY in the presence of HIA and 5-HT (top and bottom panels, respectively). (**I**) Plot of FRET intensity in response to the addition of the LBD protein. Symbols represent C8-BODIPY fluorescence at 515 nm in the presence of HIA (blue), MIA (red), or 5-HT (black).

intrinsic fluorescent intensities of the ligand at 355 nm (Figure 3G, magenta dashed line with squares). Upon the addition of the LBD protein to the mixture of MIA and C8-BODIPY, the fluorescent intensity peak of MIA at 355 nm was reduced (Figure 3F, arrow), whereas the 515 nm fluorescence of C8-BODIPY increased with red shifts in a dose-dependent manner (Figure 3F, arrowhead and inset; Figure 3G, red solid line with triangles). In the control experiments, we observed that the fluorescent intensity of C8-BODIPY alone was reduced by the addition of the LBD protein (Figure 3G, orange solid line with diamonds), probably because the hydrophobic environment around the BODIPY fluorophore was changed by the ligand binding to the Ω pocket. These FRET data allow us to conclude that MIA and C8-BODIPY simultaneously occupy the pockets (Figure 3E). We also found that HIA exhibits the similar FRET (Figure 3H, top panel; Figure 3I,

green solid line with triangles), in contrast to 5-HT, which does not show FRET (Figure 3H, bottom panel; Figure 3I, black solid line with triangles). Taken together with the above structural data, these results strongly suggest that the Ω and AF-2 pockets of PPARγ simultaneously, but individually, recognize fatty acid and indole acetate-containing ligands.

Indole acetate-containing ligands activate PPARγ in the presence of the antagonist, T0070907

To confirm whether PPARγ functionally recognizes distinct ligands through two sub-pockets, we examined the effect of the PPARγ antagonist T0070907, which covalently modifies Cys285 on the ligand-dependent receptor activation. This antagonist reportedly inhibits the receptor activation by both synthetic agonists and fatty-acid ligands (Lee et al, 2002; Shiraki et al, 2005a). In fact, the EC_{50} value of
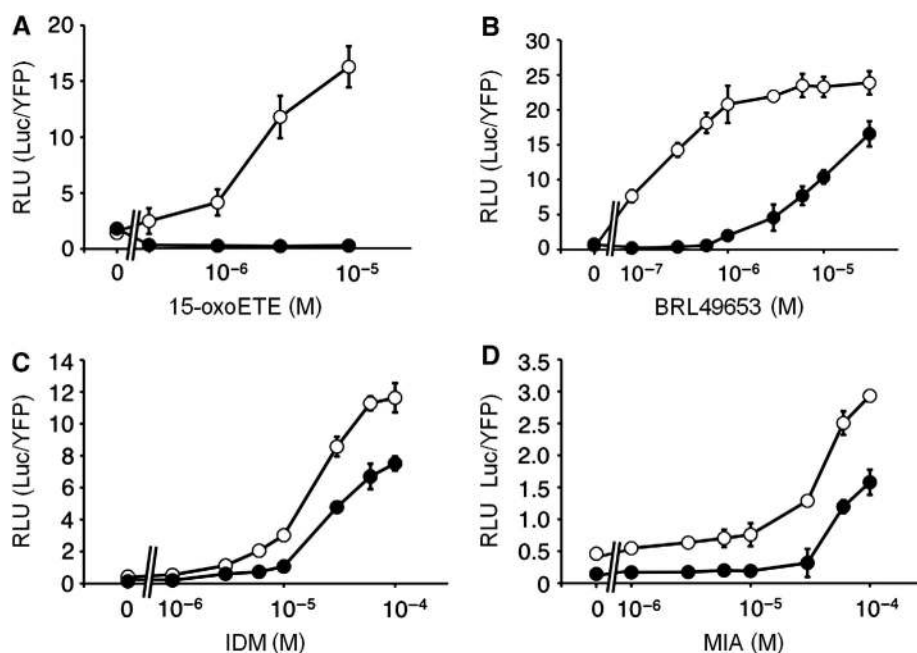
Figure 4 Effect of T0070907 on the dose-responsive transcriptional activity of Gal4DBD-PPARγLBD to various ligands. Closed and open circles represent PPARγ activities in the presence and absence of 1 μM T0070907, respectively; 15-oxoETE (**A**), BRL49653 (**B**), IDM (**C**), and MIA (**D**) were added at the final concentration indicated in each figure. The RLU (Luc/YFP) is shown with ± s.d. ($n = 4$).

15-oxoETE, which binds to the Ω pocket through the covalent modification of Cys285, was 2.89 μM in the absence of T0070907, whereas the addition of this antagonist almost completely inhibited its receptor activation (Figure 4A). Similarly, this antagonist also increased the EC_{50} value of BRL49653 from 0.17 to 12 μM (Figure 4B). This is consistent with the fact that the full agonist occupies both the AF-2 and Ω pockets to a higher extent (Figure 1B). However, the EC_{50} values for IDM, which binds to the AF-2 pocket, were not substantially affected by T0070907 (the EC_{50} values of IDM in the presence and absence of T0070907 are 28.1 and 45.7 μM, respectively; Figure 4C). Another indole acetate-containing ligand, MIA, showed an EC_{50} value of 180.3 μM in the absence of T0070907, whereas T0070907 did not antagonize the PPARγ activation by MIA, as shown with IDM, but in a different manner from that by 15-oxoETE (Figure 4D). The EC_{50} values of MIA could not be determined in the presence of the antagonist, because cellular damage was observed upon the addition of MIA at concentrations > 100 μM. These results suggest that indole acetate-containing ligands induce a distinct activation of PPARγ from that induced by fatty-acid ligands and that the former ligands are resistant to the PPARγ antagonist. Thus, we conclude that PPARγ responds differently to the two distinct ligands recognized by the AF-2 and Ω pockets.

Two ligands individually use different sites on the LBD surface to activate PPARγ

Ligand binding to the ligand-binding pocket (LBP) transmits conformational changes to the LBD surfaces, which contact the transcriptional coregulators and the heterodimer partner, thereby modulating PPARγ activity (Steinmetz *et al*, 2001). We introduced mutations into the outer LBD surface and examined their effects on receptor activation by the indole acetate-containing ligand, the fatty-acid ligand, or both of

these ligands (Figure 5A). The K301A and E471A mutants are located at the canonical coactivator-binding interface in AF-2 (Nolte *et al*, 1998). The F287A mutation is in the putative secondary coactivator-binding interface, which is mainly formed by the Ω loop (Shiraki *et al*, 2005b; Waku *et al*, 2009a). The F347A mutation resides in the heterodimer interface with the DBD of the retinoid X receptor α (RXRα) (Chandra *et al*, 2008). Immunoblot analyses of the cell lysates revealed that the expression and stability of each mutant were similar to those of the wild type (Figure 5B), suggesting that the mutations did not affect the structural integrity of the protein. Furthermore, we examined the covalent-binding ability of each mutant to 15d-PGJ$_2$ through a Michael addition, which shifted the absorption spectra of the fatty-acid ligand to shorter wavelength. As expected, each mutant showed the similar binding ability to 15d-PGJ$_2$ (Figure 5C). We then performed the cell-based reporter assay using the native promoter of the functional PPARγ-target gene, *fatty-acid-binding protein 4* (*FABP4*) (Tontonoz *et al*, 1994; Fujimoto *et al*, 2010) (Figure 5D). The BRL49653-induced activation was retained in the F287A mutant, although it was totally abolished by the F347A, K301A, and E471A mutations. The activation by the Ω pocket-specific ligands, such as 15-oxoETE and nitro-233, was somewhat sensitive, but not completely impaired by all of the mutations. In contrast, the AF-2 pocket-specific ligands, such as MIA and IDM, were resistant to the F287A and F347A mutations, but were sensitive to the K301A and E471A mutations. Thus, it is likely that the binding of ligands to the two sub-pockets individually modulates the coregulator binding and the heterodimerization through the alteration of distinct LBD surfaces, depending upon the ligand type. Notably, the combination of the two types of ligands strongly activated the wild-type receptor, in comparison with the case of a single ligand (Figure 5D, 15-oxoETE + MIA). The receptor
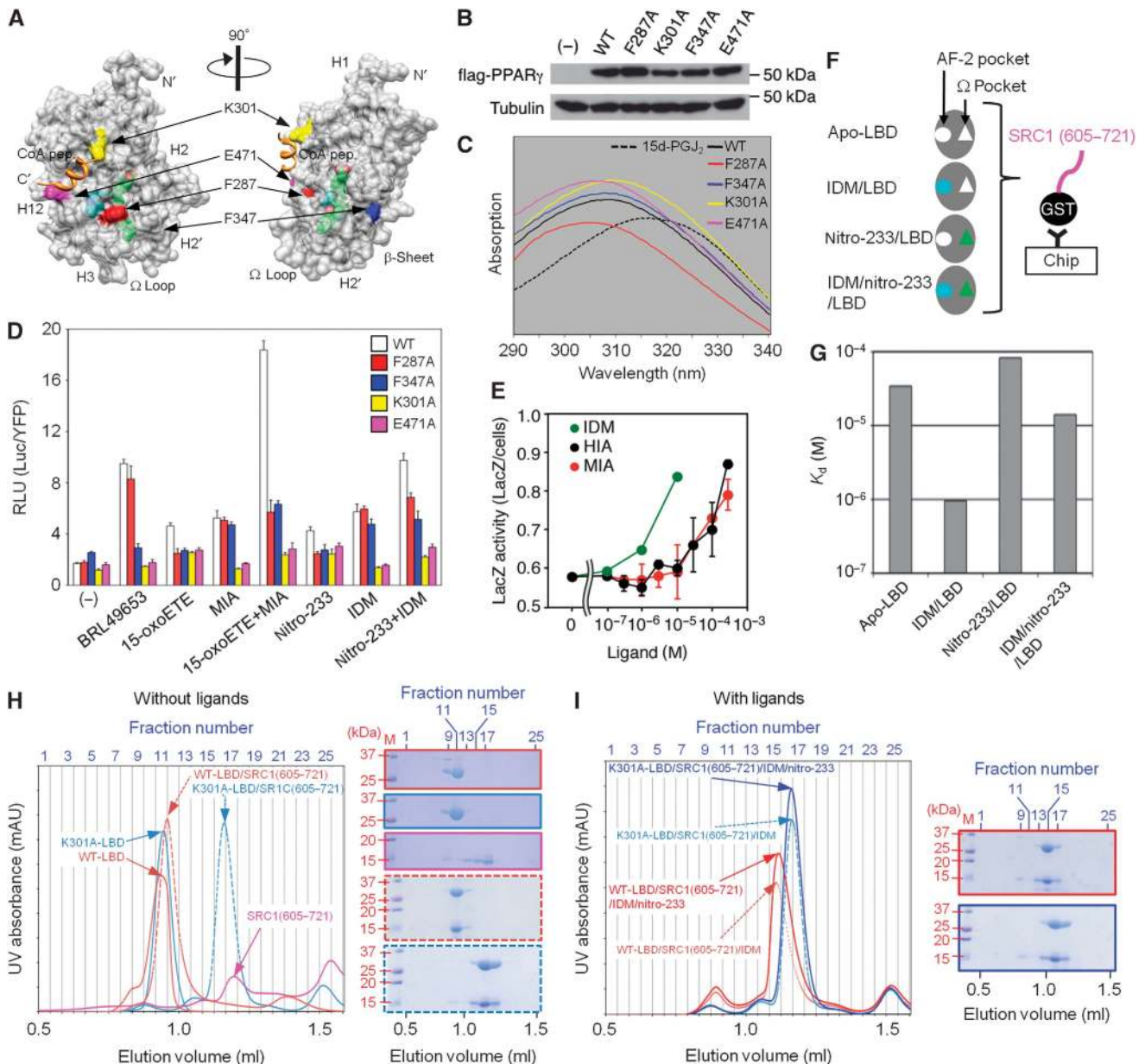
Figure 5 Requirement of the outer LBD surface in the ligand-type-specific manner for PPARγ activation. (**A**) Mapping of mutational sites on the MIA/15-oxoETE/PPARγ complex structure. The surfaces of Phe287, Phe347, Lys301, and Glu471 are coloured red, blue, yellow, and magenta, respectively. MIA and 15-oxoETE in the LBD are shown as sphere models in cyan and green, respectively. The coactivator peptide (CoA pep.), PDB code 2PARG, is superimposed and represented as an orange ribbon. (**B**) Effects of each mutation on the protein expression of flag-tagged full-length PPARγ. The wild type (WT) and each mutant were transfected into HEK293T cells. After 1 day, the cells were collected and analysed by immunoblotting with the anti-flag antibody. Mock-transfected cells (-) were used as a negative control, and tubulin was used as a reference. (**C**) Effects of each mutation on the binding ability to 15d-PGJ$_2$. 20 μM 15d-PGJ$_2$ was mixed with 20 μM wild type (WT, black line), F287A (red line), F347A (blue), K301A (yellow), or E471A LBD (magenta), respectively. The UV absorption spectra of the ligand alone (broken line) and the mixture were measured, ranging from 290 to 340 nm. (**D**) Effects of each mutation on the transcriptional activation of the *FABP4* promoter gene by full-length PPARγ. Each bar is coloured as described in (**A**). The final concentrations of BRL49653 and nitro-233 were 1 μM, 15-oxoETE and IDM were 10 μM, and MIA was 100 μM. '15-oxoETE + MIA' and 'nitro-233 + IDM' indicate the pairs of those ligands. In the top panel, the RLU (Luc/YFP) is shown with + s.d. ($n = 4$). (**E**) Ligand-dependent interaction between PPARγ and SRC1 in the yeast two-hybrid assay. The PPARγ LBD was fused to the GAL4 DBD, and the SRC1 fragment (aa 485–1441) was fused to the GAL4 AD. IDM (green), HIA (black), and MIA (red) were added at the final concentrations indicated in the figure. The lacZ activity (LacZ/cells) is shown with ± s.d. ($n = 3$) (HIA and MIA). The IDM-induced lacZ activity in each point was measured as a positive control ($n = 1$). The EC$_{50}$ values of IDM, HIA, and MIA are 4.49, 358, and 71.3 μM, respectively. (**F**, **G**) Effects of various combinations of ligands on the coactivator binding to PPARγ. (**F**) Schematic model of the SPR measurement. The GST-fused SRC1 fragment containing two LXXLL motifs (aa 605–721) was captured on the sensor chip through the anti-GST antibody, and the PPARγ LBD was injected on the sensor chip with the indicated ligand combination. (**G**) Quantitative presentation of the dissociation constants (K_d) between the SRC1 fragment and the apo-PPARγ LBD or ligand/LBD complexes. The K_d values were calculated from each sensorgram by using the kinetics tool. (**H**) Gel-filtration analyses of the PPARγ/SRC1 complex without ligands. The PPAR LBD and the SRC1 fragment (aa 605–721) were separately subjected to gel filtration (left panel, solid lines) and then the proteins within each fraction were visualized on SDS–PAGE (left panel, solid boxes). Each colour represents WT-PPARγ (red), K301A mutant (blue), or SRC1 (magenta). Dashed lines in the left panel and dashed boxes in the right panel show the PPARγ/SRC1 complex. (**I**) Gel-filtration analyses of the PPARγ/SRC1 complex with ligands. Each colour represents the WT-PPARγ/SRC1 complex (red) or the K301A-PPARγ/SRC1 complex (blue). Lines indicate the presence of both IDM and nitro-233 (solid lines), or IDM alone (dashed lines).

activation itself was sensitive to each mutation, but the inhibition patterns seemed to be dependent upon the combination of ligands. For example, the combination of nitro-233 and IDM additionally activates PPARγ, in comparison with IDM or nitro-233 alone. This cooperative activation was abolished by all four mutations, the Ω pocket-specific mutations (F287A and F347A) and the AF-2 pocket-specific ones (K301A and E471A) (Figure 5D, nitro-233 + IDM). As we did not observe any interactions between the ligands themselves within the IDM/nitro-233/PPARγLBD complex (Figure 3A; Supplementary Figure S5), this cooperative activation should be induced by coregulator binding.

In fact, the indole acetate-containing ligands, IDM, HIA, and MIA, induced the interaction between the SRC1 fragment containing four LXXLL motifs (aa 485–1441) and the PPARγ LBD in a dose-dependent manner, as shown in the yeast two-hybrid system (Figure 5E). We also confirmed, using various deletion mutants of SRC1, that the central region containing three LXXLL motifs (L1–3; aa 544–897) mainly functions in the interaction with the PPARγ LBD (Supplementary Figure S6). Thus, we performed SPR measurements to examine the dissociation constant of coactivator binding (Figure 5F). The SPR signals showed slow binding and dissociation, even in the absence of ligands (Supplementary Figure S7), and the dissociation constant was calculated to be 34.2 μM (Figure 5G, lane 1). In the presence of IDM, the dissociation became slower and the K_d value changed to 0.96 μM (lane 2). Unexpectedly, nitro-233 induced faster dissociation of the complex ($K_d = 82.7$ μM, lane 3), and the addition of IDM to nitro-233 seemed to mix their effects ($K_d = 14.1$ μM, lane 4), indicating that the cooperation between two ligands cannot be simply explained by the strength of the coactivator binding. Although this study has not provided information about the factors targeting for the Phe287 surface, it is likely that this residue discriminates the coregulator binding specifically for fatty-acid ligands (Figure 5D).

Activation mechanism of PPARγ by two ligands

To examine the ligand-type-specific effects on the conformational alteration of the coactivator/PPARγ LBD complex, we performed gel-filtration analyses of the PPARγ LBD/SRC1 complex and visualized the proteins within each fraction by SDS–PAGE. We observed that the WT-LBD mixed with the SRC1 fragment (aa 605–721) migrated slower than the LBD alone, even in the absence of ligands (Figure 5H, red dashed box), indicating that they interact with each other in a ligand-independent manner, as described previously (Molnár *et al*, 2005). This is consistent with the data from the SPR experiment (Supplementary Figure S7; Figure 5G), showing that the apo-form of the WT-LBD binds to the SRC1 fragment in a two-state reaction model, rather than a 1:1 binding model. The addition of IDM to the WT-LBD/SRC1 caused slower migration, as observed by their elution volume (Figure 5I, red dashed line). It is generally accepted that the migration speeds of proteins in gel filtration depend upon their molecular shapes (Stokes radius) in addition to their sizes (Erickson, 2009), suggesting that IDM binding induces conformational alterations of the WT-LBD/SRC1 complex.

Similarly to the wild type, the K301A mutant also formed the complex with SRC1 in the absence of ligands (Figure 5H, blue dashed box). However, the elution volume was different from that of the WT-LBD/SRC1 complex (Figure 5H, dashed

lines), implying that the complex molecule adopt a distinct shape. Meanwhile, the migration speed of the K301A/SRC1 complex was not altered by the addition of IDM (Figure 5I, blue lines), suggesting that the K301A mutation blocks the structural alteration of the complex by the indole acetate-containing ligand. Notably, the elution volume of the WT-LBD/SRC1/IDM complex was significantly different from that of the K301A/SRC1/IDM complex (Figure 5I, dashed lines), suggesting that they have distinct conformations. Intriguingly, nitro-233 did not induce any alterations in the complex (Figure 5I, solid lines). These results allowed us to presume that the binding of the Ω pocket-specific ligands may affect other coregulators than SRC1 (aa 605–721) to activate PPARγ. Thus, the cooperativity of the two ligands has not been completely explained by the coactivator binding alone. At the moment, we assume that the two ligands individually regulate coactivation and/or anti-repression to activate PPARγ (see Discussion for details).

Considerable evidence exists to support the specific receptor-independent action of 5-HT (Srinivasan *et al*, 2008), and hence we examined whether the 5-HT metabolites might be mediators of this function. Immunoblot analyses revealed that MAO proteins were expressed in PMA-activated THP-1 cells (Figure 6A, lane 1) and were not affected by the SERT inhibitor, Citalopram, or the MAO inhibitor, Harmine (Figure 6A, lanes 3 and 4). We found that the endogenous FABP4 protein was up-regulated by the application of 5-HT to PMA-treated THP-1 cells (Figure 6B, lanes 1 and 2). In contrast, this effect was completely inhibited by Citalopram (Figure 6B, lanes 3 and 4) and by Harmine (Figure 6B, lanes 7 and 8). 5-HT did not activate PPARγ in HEK293T cells, because they lack any MAO isoforms (Figure 6A, lane 5), consistent with the previous report (Vindis *et al*, 2001). These results suggest that the 5-HT-induced FABP4 expression is dependent on the 5-HT uptake and catabolism. Thus, PPARγ may function as a multiple sensor for both 5-HT and fatty-acid metabolism in cells (Figure 6C).

Discussion

Structural insights into the integration of PPARγ agonisms by synthetic and endogenous ligands

Through continuous efforts to develop more effective drugs, selective PPARγ modulators were designed as partial agonists, which induced weaker activation of the receptor than the full agonists, through the non-AF-2-mediated agonism. Meanwhile, we previously reported that fatty-acid ligands display a distinct type of agonism through the covalent modification with Cys285 and the conformational alteration of the Ω loop (Shiraki *et al*, 2005a; Waku *et al*, 2009a, b). Thus, the PPARγ agonism is a quite interesting issue with many open questions (Moras, 2008). This work is the first to identify 5-HT metabolites as endogenous PPARγ ligands interacting with AF-2, and we have proposed a novel agonism, in which 5-HT and/or fatty-acid metabolites specifically bind to two sub-pockets partitioned by Cys285 and Met364 (Figure 6C, see the figure legend for details).

Our crystal structures of the complexes with the ligands validated the ligand-binding mode in the Y-shaped LBP. Intriguingly, both MIA and 15oxoETE adopt various configurations among the MIA, 15-oxoETE, and MIA/15-oxoETE complexes (Supplementary Figure S8A); MIA interacts with
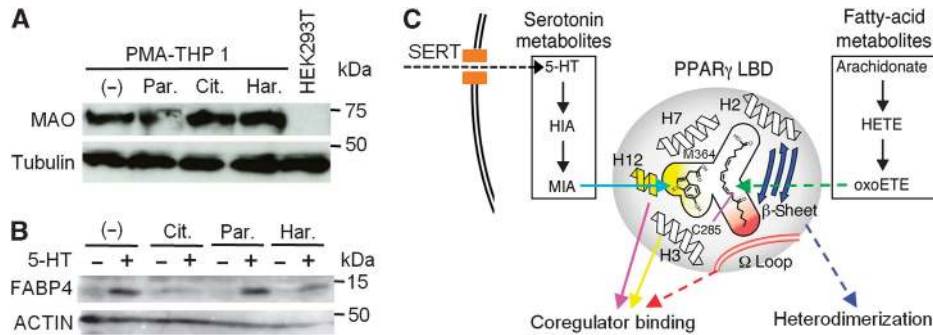
Figure 6 Possible crosstalk between 5-HT metabolism and PPARγ activation. (**A**) Effects of the SERT and the MAO inhibitors on MAO expression in PMA-activated THP-1 cells. Cells were treated with PMA, and subsequently with the indicated inhibitors. The concentration of each drug was 0.1 µM. HEK293T cells were used as the negative control for the immunoblot. Tubulin was used as a reference. (**B**) Effects of the SERT or MAO inhibitor on FABP4 expression in PMA-activated THP-1 cells. After the activation by PMA, the cells were treated with (+) or without (−) 500 µM 5-HT, combined with Citalopram (Cit.), Paroxetine (Par.), or Harmine (Har.) at a final concentration of 0.1 µM. ACTIN was used as a reference. (**C**) Schematic model of the PPARγ activation mechanism dependent upon either serotonin metabolism or fatty-acid metabolism. PPARγ possesses a Y-shaped LBP (the area enclosed by the black solid line), which is divided into two sub-pockets by Cys285 and Met364. Extracellular 5-HT is incorporated into cells by the SERT (black dashed line), and then catabolized to MIA (the left box). The 5-HT metabolite binds to the AF-2 pocket (yellow area), and modulates the AF-2-mediated coregulator binding through the charge clamp (Lys301 on helix H3 and Glu471 on helix H12) (yellow and purple solid arrows). On the other hand, fatty-acid metabolites, bound to the Ω pocket (red area), modulate the coregulator binding through the Ω loop (red dashed arrow), and the heterodimerization with RXRα through the β-sheet (blue dashed arrows). MIA and 15-oxoETE are schematically shown as representatives of serotonin and fatty-acid metabolites, respectively. The covalent modification of Cys285 with 15-oxoETE is shown as a purple solid line.

Tyr473 through its carboxyl group in the MIA complex (magenta), whereas Tyr473 forms a direct interaction through the nitrogen in the MIA/15-oxoETE complexes (cyan). In contrast, few differences in the ligand configurations were observed in the complexes with the mimetic agonists (Supplementary Figure S8B). This finding indicates that the configurations of the endogenous ligands are versatile, whereas those of the synthetic agonists are relatively invariant within the specialized sub-pockets. On the other hand, mutagenesis experiments revealed that the MIA-dependent activation requires the AF-2 interface, modulated by the direct interaction between the ligand and Tyr473, in the presence or absence of 15-oxoETE (Figure 5D). Although this study has not clarified the effects of the different interactions between MIA and Tyr473 on the PPARγ activation, these results suggest that the interactions between the endogenous ligands and AF-2 are at least adaptable, regardless of the ligand binding in the Ω pocket and are essential for the ligand-dependent activation of PPARγ.

Furthermore, we observed that two ligands jointly induce the PPARγ activation more strongly than each ligand alone in the cell-based reporter assay. This cooperative activation was not observed in the adipogenesis experiment of 3T3-L1 cells (Supplementary Figure S9A; IDM/nitro-233). This could be explained by the following model (Supplementary Figure S9B): the covalent binding with 15-oxoETE induces anti-repression, which is coupled with a local structural change around Phe287. In response to indole acetate-containing ligands, the receptor uses the charge clamp (Lys301 and Glu471) to induce conformational changes of the coactivators, thereby leading to full activation. When the charge clamp is impaired, the coactivators can no longer bind to the AF-2 interface of PPARγ LBD, and hence the activation is blocked. As the coactivators themselves may induce anti-repression independently of the covalent binding of ligands in the Ω pocket, certain types of cells, such as adipocytes, would be insensitive to partial agonists. In fact,

we found that IDM induces adipocyte differentiation, whereas nitro-233 does not (Supplementary Figure S9A), implying that this model might address the tissue-specific action of partial agonists. Our current knowledge cannot fully explain the relationships between the PPARγ activity in cells and the coactivator binding (Figure 5). Thus, a complete understanding of the cooperative action of two ligands will await future studies focusing on the mechanism of coregulator bindings coupled with the PPARγ agonism.

Physiological aspects and pharmacological impacts of PPARγ as a multiple sensor for 5-HT and fatty-acid metabolites

5-HT is present at high levels within the gastrointestinal (GI) tract, as well as the central nervous system (Gershon and Tack, 2007). Within the GI tract, 5-HT is synthesized and released to the plasma at a micromolar concentration per minute (Dunlop et al, 2005). Our data suggest that the plasma 5-HT within the GI tract may be incorporated into macrophages by the SERT, and then its MAO-mediated metabolites act on PPARγ (Figure 6B). Treatments with PPARγ agonists improve experimental colitis (Auwerx, 2002; Bull, 2003), and abnormal 5-HT metabolism causes GI pathology, such as irritable bowel disease and colorectal polyposis (Costedio et al, 2007). Accordingly, the data presented in this work imply that the 5-HT-PPARγ pathway may illuminate the causes of these diseases, thereby leading to appropriate drug treatments. In addition to its physiological functions within the GI tract, plasma 5-HT also regulates the bone mass and cardiac function (Dempsie and MacLean, 2008; Fligny et al, 2008; Yadav et al, 2010), which are both reported as the pharmacological effects of full PPARγ agonists (Nissen and Wolski, 2007; Grey, 2009). Thus, our findings of crosstalk between 5-HT metabolism and PPARγ will extend beyond the physiological function of PPARγ in obesity.

Furthermore, our results that 5-HT metabolites acts on PPARγ may provide three possible impacts on the drug

development, such as (i) structural discrimination of the two main effects of an non-steroidal anti-inflammatory drugs (NSAIDs) on COX inhibition and PPARγ activation, (ii) novel serotonergic signalling, and (iii) reconsideration of antagonist effects and indirect modulation of PPARγ. (i) The COX inhibitor IDM is clinically used as an NSAID (Mitchell et al, 1994; Shiff and Rigas, 1999). It was reported that the pharmacological efficiencies of IDM could be attributed to its ability to adopt a range of different conformers, defined by the torsion angle (ϕ) of the imido bond between the chlorobenzene and indole rings (Hori et al, 2006). In our structure, IDM functionally binds to the AF-2 pockets at $\phi = 75°$ (Figure 1E), in contrast to $\phi = -59°$ in COX-2 (PDB 4COX: Kurumbail et al, 1996). This structural data may represent a milestone in the development of an NSAID that discriminates between COX inhibition and PPARγ activation. In fact, IDM analogues with different ϕ angles reduced the COX activity and the cell toxicity, but induced the PPARγ-dependent adipogenesis (Felts et al, 2007). (ii) Imbalances in the 5-HT levels within the GI tract have been observed in patients with chronic inflammatory bowel syndrome-like symptoms, such as ulcerative colitis and Crohn's disease (Costedio et al, 2007). Some symptoms can be explained by 5-HT receptors, but the peripheral effects of 5-HT uptake inhibitors have remained obscure. For example, SERT inhibitors are effective in the treatment of insulin sensitivity in obese patients in addition to anxiety (Lustman and Clouse, 2005), but the pathways regulated by 5-HT signalling have not been defined (Costedio et al, 2007). Interestingly, a mutation in SERT (mod-5) in Caenorhabditis elegans affected insulin and nuclear receptor signalling independently of serotonergic receptors, resulting in the dysregulation of fat metabolism (Liang et al, 2006; Srinivasan et al, 2008). Our results suggest that 5-HT metabolites may mediate the above novel functions through PPARγ. As obesity is a major public health problem, this possibility should be experimentally clarified in the future. (iii) Unlike the classical agonists, the indole acetate-containing ligands activate PPARγ even in the presence of the PPARγ antagonist, T0070907 (Figure 4), thus suggesting a need to reconsider the pharmacologically and genetically controversial issues of PPARγ-mediated and non-mediated phenomena, such as neuroprotection from Aβ (Sagi et al, 2003) and GI polyp formation (Lefebvre et al, 1998; Saez et al, 1998; Sarraf et al, 1998; Niho et al, 2003).

Materials and methods

Protein preparation and X-ray crystallography of the ligand/LBD complex

The human PPARγ LBD (aa 203–477) was purified as described previously (Waku et al, 2009a). To avoid confusion because of differences in crystal packing, all crystals were prepared through co-crystallization with the relevant ligand under the same conditions. A 2 µl aliquot of protein solution (15 mg/ml in 20 mM Tris, pH 8.0, 150 mM NaCl) was mixed with an equal volume of 0.1 mM ligand solution (0.8 M sodium citrate, 100 mM HEPES, pH 7.5, 1% DMSO), and then the ligand/protein mixture was co-crystallized without co-purification, by the hanging drop vapour diffusion method at 293 K. All complex crystals were flash cooled in a liquid nitrogen stream, after briefly soaking them in cryoprotection buffer (1.1 M sodium citrate, 100 mM HEPES, pH 7.5, and 25% (v/v) glycerol). Diffraction data were collected at BL38B1 in SPring-8 (Harima, Japan). All data were processed using HKL2000 (Otwinowski and Minor, 1997). All structures were solved by the molecular replacement method, using the previously published structure of the apo-hPPARγ LBD

(PDB 1PRG) as a search model (Nolte et al, 1998). The correctly positioned molecules were refined with CNS (Brünger et al, 1998) and O (Jones et al, 1991). The crystallographic data and refinement statistics are summarized in Table S1.

Discrimination of structural figures

All crystals determined in this study display the symmetry of the space group *C2*, and contain two LBD molecules, chains A and B, within the asymmetric unit (Supplementary Figure S2). In the LBD structures in complex with IDM, HIA, MIA, or 5-HT alone, the Ω loop in chain A was not built, because of disordered structures (Supplementary Figure S2A–D). In several cases, ligands were observed in chain B (Supplementary Figure S2H–M). However, their helix H12 and AF-2 pocket were frequently disoriented, depending upon the crystal packing (Waku et al, 2009a). Accordingly, we omitted chain B and the ligands from the figures for structural comparison. As for the average *B*-factors of IDM and MIA, the molecules in the AF-2 pocket within chain A exhibit the lowest *B*-factors among chains A and B (Supplementary Figures S2H–J, S3B and C), in good agreement with the conclusion in the text.

Cell-based reporter assay

Relevant plasmids were introduced into HEK293T cells, using a CellPhect Transfection kit (GE Healthcare) according to the manufacturer's instructions. After 24 h, various ligands were added to the cells at the indicated concentrations. The yellow fluorescence protein (YFP) intensity and the Luciferase (Luc) activity were then analysed after 24 h using Fusion α (Packard Bioscience). The relative luminescence unit (RLU) represents the Luc value normalized to the YFP intensity (Luc/YFP) and the error bar is the s.d.

SPR analysis

SPR measurements were performed using a Biacore X100 at 24°C. For SPR experiments to determine the dissociation constant between the PPARγ LBD and IDM or 5-HT metabolites (Supplementary Figure S1B–E), the his-PPARγ LBD proteins were immobilized on the Sensor chip NTA (GE Healthcare) bound with nickel. Experiments were performed by injecting each ligand, at a flow rate of 30 µl/min. Binding was measured in the following order: the blank and the his-PPARγ LBD. Between experiments for each ligand, the sensor chip was regenerated by using EDTA and NaOH. For SPR experiments to determine the dissociation constant between the PPARγ LBD and the coactivator SRC1 (Figure 5G), we used an anti-GST antibody immobilized onto the Sensor chip CM5 (GE Healthcare). The SRC1 fragment (aa 605–721) was expressed using pGEX-4T vector (GE Healthcare) into Escherichia coli BL21 (DE3) and was purified by chromatography on GSTrap (5 ml CV) and Q HP (5 ml CV) columns (GE Healthcare). The GST-fused SRC1 fragment (aa 605–721) was captured by the chip, and the PPARγ LBD was injected with or without ligands (Figure 5F). Between experiments for each assay, the sensor chip was regenerated by using 10 mM glycine pH 2.0. Data were collected in the single-kinetics mode and dissociation constants were analysed by the kinetics tool.

FRET-based ligand-binding assay

C8-BODIPY (final concentration, 1 µM) was mixed with MIA (final concentration, 2 µM). A small aliquot of the LBD protein was then added to the cuvette to achieve the indicated final concentrations, as described in the legend to Figure 3F–I. The fluorescence spectrum of each mixture was measured with an excitation wavelength of 290 nm at 20°C, by using a HITACHI fluorescent spectrometer F-4500. Emission spectra from 300 to 540 nm were recorded. The excitation and emission slits were set to 2.5 and 1.0 mm, respectively. When the fluorescent spectra of C8-BODIPY alone were measured as a control for FRET, the excitation wavelength was changed to 480 nm.

Gel-filtration experiment

The SRC1 fragment (aa 605–721) was expressed using the pGEX-4T vector (GE Healthcare) in E. coli BL21 (DE3) and was purified by chromatography on GSTrap (5 ml CV) and Q HP (5 ml CV) columns (GE Healthcare). For gel filtration, the GST tag was digested and removed from the SRC1 fragment. To prepare the complex sample, 0.1 mM PPARγ LBD and 0.1 mM SRC1 (aa 605–721) fragment were incubated with 10 mM IDM and 2 mM nitro-233 on ice for 30 min, and then 40 µl samples were injected into a Superdex 75 PC 3.2/30

column (GE Healthcare) mounted on a SMART system (Pharmacia). The absorbance at 280 nm was recorded.

Supplementary data

Supplementary data are available at *The EMBO Journal* Online (http://www.embojournal.org).

Acknowledgements

Conflict of interest

The authors declare that they have no conflict of interest.

References

Artis DR, Lin JJ, Zhang C, Wang W, Mehra U, Perreault M, Erbe D, Krupka HI, England BP, Arnold J, Plotnikov AN, Marimuthu A, Nguyen H, Will S, Signaevsky M, Kral J, Cantwell J, Settachatgull C, Yan DS, Fong D *et al* (2009) Scaffold-based discovery of indeglitazar, a PPAR pan-active anti-diabetic agent. *Proc Natl Acad Sci USA* **106:** 262–267

Auwerx J (2002) Nuclear receptors. I. PPAR gamma in the gastrointestinal tract: gain or pain? *Am J Physiol Gastrointest Liver Physiol* **282:** G581–G585

Berger JP, Akiyama TE, Meinke PT (2005) PPARs: therapeutic targets for metabolic disease. *Trends Pharmacol Sci* **26:** 244–251

Brünger AT, Adams PD, Clore GM, DeLano WL, Gros P, Grosse-Kunstleve RW, Jiang JS, Kuszewski J, Nilges M, Pannu NS, Read RJ, Rice LM, Simonson T, Warren GL (1998) Crystallography & NMR system: a new software suite for macromolecular structure determination. *Acta Crystallogr D Biol Crystallogr* **54:** 905–921

Bruning JB, Chalmers MJ, Prasad S, Busby SA, Kamenecka TM, He Y, Nettles KW, Griffin PR (2007) Partial agonists activate PPARγ using a helix 12 independent mechanism. *Structure* **15:** 1258–1271

Bull AW (2003) The role of peroxisome proliferator-activated receptor γ in colon cancer and inflammatory bowel disease. *Arch Pathol Lab Med* **127:** 1121–1123

Chandra V, Huang P, Hamuro Y, Raghuram S, Wang Y, Burris TP, Rastinejad F (2008) Structure of the intact PPAR-γ-RXR-α nuclear receptor complex on DNA. *Nature* **456:** 350–356

Ceriello A (2008) Thiazolidinediones as anti-inflammatory and anti-atherogenic agents. *Diabetes Metab Res Rev* **24:** 14–26

Costedio MM, Hyman N, Mawe GM (2007) Serotonin and its role in colonic function and in gastrointestinal disorders. *Dis Colon Rectum* **50:** 376–388

Cronet P, Petersen JF, Folmer R, Blomberg N, Sjöblom K, Karlsson U, Lindstedt EL, Bamberg K (2001) Structure of the PPARα and -γ ligand binding domain in complex with AZ 242; ligand selectivity and agonist activation in the PPAR family. *Structure* **9:** 699–706

Dempsie Y, MacLean MR (2008) Pulmonary hypertension: therapeutic targets within the serotonin system. *Br J Phamacol* **155:** 455–462

Dunlop SP, Coleman NS, Blackshaw E, Perkins AC, Singh G, Marsden CA, Spiller RC (2005) Abnormalities of 5-hydroxytryptamine metabolism in irritable bowel syndrome. *Clin Gastroenterol Hepatol* **3:** 349–357

Erickson HP (2009) Size and shape of protein molecules at the nanometer level determined by sedimentation, gel filtration, and electron microscopy. *Biological Protocol Online*, Shulin Li (ed) pp 32–51

Evans RM, Barish GD, Wang YX (2004) PPARs and the complex journey to obesity. *Nat Med* **10:** 355–361

Felts AS, Ji C, Stafford JB, Crews BC, Kingsley PJ, Rouzer CA, Washington MK, Subbaramaiah K, Siegel BS, Young SM, Dannenberg AJ, Marnett LJ (2007) Desmethyl derivatives of indomethacin and sulindac as probes for cyclooxygenase-dependent biology. *ACS Chem Biol* **2:** 479–483

Fligny C, Fromes Y, Bonnin P, Darmon M, Bayard E, Launay JM, Côté F, Mallet J, Vodjdani G (2008) Maternal serotonin influences cardiac function in adult offspring. *FASEB J* **22:** 2340–2349

Fontana E, Boucher J, Marti L, Lizcano JM, Testar X, Zorzano A, Carpéné C (2001) Amine oxidase substrates mimic several of the insulin effects on adipocyte differentiation in 3T3 F442A cells. *Biochem J* **356:** 769–777

Forman BM, Tontonoz P, Chen J, Brun RP, Spiegelman BM, Evans RM (1995) 15-deoxy-$\Delta^{12,14}$-prostaglandin J$_2$ is a ligand for the adipocyte determination factor PPARγ. *Cell* **83:** 803–812

Fuemmeler BF, Agurs-Collins TD, McClernon FJ, Kollins SH, Kail ME, Bergen AW, Ashley-Koch AE (2008) Genes implicated in serotonergic and dopaminergic functioning predict BMI categories. *Obesity* **16:** 348–355

Fujimoto Y, Shiraki T, Horiuchi Y, Waku T, Shigenaga A, Otaka A, Ikura T, Igarashi K, Aimoto S, Tate S, Morikawa K (2010) Proline cis/trans isomerase Pin1 regulates peroxisome proliferator-activated receptor γ activity through the direct binding to the AF-1 domain. *J Biol Chem* **285:** 3126–3132

Gampe Jr RT, Montana VG, Lambert MH, Miller AB, Bledsoe RK, Milburn MV, Kliewer SA, Willson TM, Xu HE (2000) Asymmetry in the PPARγ/RXRα crystal structure reveals the molecular basis of heterodimerization among nuclear receptors. *Mol Cell* **5:** 545–555

Gershon MD, Tack J (2007) The serotonin signaling system: from basic understanding to drug development for functional GI disorders. *Gastroenterology* **132:** 397–414

Grey A (2009) Thiazolidinedione-induced skeletal fragility—mechanisms and implications. *Diabetes Obes Metab* **11:** 275–284

Hori T, Ishijima J, Yokomizo T, Ago H, Shimizu T, Miyano M (2006) Crystal structure of anti-configuration of indomethacin and leukotriene B$_4$ 12-hydroxydehydrogenase/15-oxo-prostaglandin 13-reductase complex reveals the structural basis of broad spectrum indomethacin efficacy. *J Biochem* **140:** 457–466

Huang JT, Welch JS, Ricote M, Binder CJ, Willson TM, Kelly C, Witztum JL, Funk CD, Conrad D, Glass CK (1999) Interleukin-4-dependent production of PPAR-γ ligands in macrophages by 12/15-lipoxygenase. *Nature* **400:** 378–382

Itoh T, Fairall L, Amin K, Inaba Y, Szanto A, Balint BL, Nagy L, Yamamoto K, Schwabe JW (2008) Structural basis for the activation of PPARγ by oxidized fatty acids. *Nat Struct Mol Biol* **15:** 924–931

Jones TA, Zou JY, Cowan SW, Kjeldgaard M (1991) Improved methods for building protein models in electron density maps and the location of errors in these models. *Acta Cryst A* **47:** 110–119

Kliewer SA, Lenhard JM, Willson TM, Patel I, Morris DC, Lehmann JM (1995) A prostaglandin J$_2$ metabolite binds peroxisome proliferator-activated receptor γ and promotes adipocyte differentiation. *Cell* **83:** 813–819

Kurumbail RG, Stevens AM, Gierse JK, McDonald JJ, Stegeman RA, Pak JY, Gildehaus D, Miyashiro JM, Penning TD, Seibert K, Isakson PC, Stallings WC (1996) Structural basis for selective inhibition of cyclooxygenase-2 by anti-inflammatory agents. *Nature* **384:** 644–648

Laffitte BA, Joseph SB, Walczak R, Pei L, Wilpitz DC, Collins JL, Tontonoz P (2001) Autoregulation of the human liver X receptor α promoter. *Mol Cell Biol* **21:** 7558–7568

Lee G, Elwood F, McNally J, Weiszmann J, Lindstrom M, Amaral K, Nakamura M, Miao S, Cao P, Learned RM, Chen JL, Li Y (2002) T0070907, a selective ligand for peroxisome proliferator-activated receptor γ, functions as an antagonist of biochemical and cellular activities. *J Biol Chem* **277:** 19649–19657

Lefebvre AM, Chen I, Desreumaux P, Najib J, Fruchart JC, Geboes K, Briggs M, Heyman R, Auwerx J (1998) Activation of the peroxisome proliferator-activated receptor γ promotes the development of colon tumors in C57BL/6J-APCMin/+ mice. *Nat Med* **4:** 1053–1057

Lehmann JM, Lenhard JM, Oliver BB, Ringold GM, Kliewer SA (1997) Peroxisome proliferator-activated receptors α and γ are activated by indomethacin and other non-steroidal anti-inflammatory drugs. *J Biol Chem* **272:** 3406–3410

Lehrke M, Lazar MA (2005) The many faces of PPARγ. *Cell* **123:** 993–999

Li Y, Lambert MH, Xu HE (2003) Activation of nuclear receptors: a perspective from structural genomics. *Structure* **11:** 741–746

Liang B, Moussaif M, Kuan CJ, Gargus JJ, Sze JY (2006) Serotonin targets the DAF-16/FOXO signaling pathway to modulate stress responses. *Cell Metab* **4:** 429–440

Lustman PJ, Clouse RE (2005) Depression in diabetic patients: the relationship between mood and glycemic control. *J Diabetes Complications* **19:** 113–122

Mahindroo N, Huang CF, Peng YH, Wang CC, Liao CC, Lien TW, Chittimalla SK, Huang WJ, Chai CH, Prakash E, Chen CP, Hsu TA, Peng CH, Lu IL, Lee LH, Chang YW, Chen WC, Chou YC, Chen CT, Goparaju CM et al (2005) Novel indole-based peroxisome proliferator-activated receptor agonists: design, SAR, structural biology, and biological activities. *J Med Chem* **48:** 8194–8208

Marcus SL, Miyata KS, Zhang B, Subramani S, Rachubinski RA, Capone JP (1993) Diverse peroxisome proliferator-activated receptors bind to the peroxisome proliferator-responsive elements of the rat hydratase/dehydrogenase and fatty acyl-CoA oxidase genes but differentially induce expression. *Proc Natl Acad Sci USA* **90:** 5723–5727

McKenna NJ, Cooney AJ, DeMayo FJ, Downes M, Glass CK, Lanz RB, Lazar MA, Mangelsdorf DJ, Moore DD, Qin J, Steffen DL, Tsai MJ, Tsai SY, Yu R, Margolis RN, Evans RM, O'Malley BW (2009) Minireview: evolution of NURSA, the Nuclear Receptor Signaling Atlas. *Mol Endocrinol* **26:** 740–746

Mitchell JA, Akarasereenont P, Thiemermann C, Flower RJ, Vane JR (1994) Selectivity of nonsteroidal antiinflammatory drugs as inhibitors of constitutive and inducible cyclooxygenase. *Proc Natl Acad Sci USA* **90:** 11693–11697

Molnár F, Matilainen M, Carlberg C (2005) Structural determinants of the agonist-independent association of human peroxisome proliferator-activated receptors with coactivators. *J Biol Chem* **280:** 26543–26556

Montanari R, Saccoccia F, Scotti E, Crestani M, Godio C, Gilardi F, Loiodice F, Fracchiolla G, Laghezza A, Tortorella P, Lavecchia A, Novellino E, Mazza F, Aschi M, Pochetti G (2008) Crystal structure of the peroxisome proliferator-activated receptor γ (PPARγ) ligand binding domain complexed with a novel partial agonist: a new region of the hydrophobic pocket could be exploited for drug design. *J Med Chem* **51:** 7768–7776

Moras D (2008) Structure of full-length PPARγ-RXRα: a snapshot of a functional complex? *Cell Metab* **9:** 8–10

Nagy L, Schwabe JW (2004) Mechanism of the nuclear receptor molecular switch. *Trends Biochem Sci* **29:** 317–324

Niho N, Takahashi M, Kitamura T, Shoji Y, Itoh M, Noda T, Sugimura T, Wakabayashi K (2003) Concomitant suppression of hyperlipidemia and intestinal polyp formation in Apc-deficient mice by peroxisome proliferator-activated receptor ligands. *Cancer Res* **63:** 6090–6095

Nissen SE, Wolski K (2007) Effect of rosiglitazone on the risk of myocardial infarction and death from cardiovascular causes. *N Engl J Med* **14:** 2457–2471

Nolte RT, Wisely GB, Westin S, Cobb JE, Lambert MH, Kurokawa R, Rosenfeld MG, Willson TM, Glass CK, Milburn MV (1998) Ligand binding and co-activator assembly of the peroxisome proliferator-activated receptor-γ. *Nature* **395:** 137–143

Oberfield JL, Collins JL, Holmes CP, Goreham DM, Cooper JP, Cobb JE, Lenhard JM, Hull-Ryde EA, Mohr CP, Blanchard SG, Parks DJ, Moore LB, Lehmann JM, Plunket K, Miller AB, Milburn MV, Kliewer SA, Willson TM (1999) A peroxisome proliferator-activated receptor γ ligand inhibits adipocyte differentiation. *Proc Natl Acad Sci USA* **96:** 6102–6106

Odegaard JI, Ricardo-Gonzalez RR, Goforth MH, Morel CR, Subramanian V, Mukundan L, Red Eagle A, Vats D, Brombacher F, Ferrante AW, Chawla A (2007) Macrophage-specific PPARγ controls alternative activation and improves insulin resistance. *Nature* **447:** 1116–1120

Otwinowski Z, Minor W (1997) Processing of X-ray diffraction data collected in oscillation mode. *Method Enzymol* **276:** 307–326

Pochetti G, Godio C, Mitro N, Caruso D, Galmozzi A, Scurati S, Loiodice F, Fracchiolla G, Tortorella P, Laghezza A, Lavecchia A, Novellino E, Mazza F, Crestani M (2007) Insights into the mechanism of partial agonism: crystal structures of the peroxisome proliferator-activated receptor γ ligand-binding domain in the complex with two enantiomeric ligands. *J Biol Chem* **282:** 17314–17324

Reginato MJ, Bailey ST, Krakow SL, Minami C, Ishii S, Tanaka H, Lazar MA (1998) A potent antidiabetic thiazolidinedione with unique peroxisome proliferator-activated receptor γ-activating properties. *J Biol Chem* **273:** 32679–32684

Ricote M, Li AC, Willson TM, Kelly CJ, Glass CK (1998) The peroxisome proliferator-activated receptor-γ is a negative regulator of macrophage activation. *Nature* **391:** 79–82

Saez E, Tontonoz P, Nelson MC, Alvarez JG, Ming UT, Baird SM, Thomazy VA, Evans RM (1998) Activators of the nuclear receptor PPARγ enhance colon polyp formation. *Nat Med* **4:** 1058–1061

Sagi SA, Weggen S, Eriksen J, Golde TE, Koo EH (2003) The non-cyclooxygenase targets of non-steroidal anti-inflammatory drugs, lipoxygenases, peroxisome proliferator-activated receptor, inhibitor of κB kinase, and NF κB, do not reduce amyloid β42 production. *J Biol Chem* **278:** 31825–31830

Sarraf P, Mueller E, Jones D, King FJ, DeAngelo DJ, Partridge JB, Holden SA, Chen LB, Singer S, Fletcher C, Spiegelman BM (1998) Differentiation and reversal of malignant changes in colon cancer through PPARγ. *Nat Med* **4:** 1046–1052

Schopfer FJ, Lin Y, Baker PR, Cui T, Garcia-Barrio M, Zhang J, Chen K, Chen YE, Freeman BA (2005) Nitrolinoleic acid: an endogenous peroxisome proliferator-activated receptor γ ligand. *Proc Natl Acad Sci USA* **102:** 2340–2345

Shiraki T, Kamiya N, Shiki S, Kodama TS, Jingami H (2005a) α,β-unsaturated ketone is a core moiety of natural ligands for covalent binding to peroxisome proliferator-activated receptor γ. *J Biol Chem* **280:** 14145–14153

Shiraki T, Kodama TS, Jingami H, Kamiya N (2005b) Rational discovery of a novel interface for a coactivator in the peroxisome proliferator-activated receptor γ: theoretical implications of impairment in type 2 diabetes mellitus. *Proteins* **58:** 418–425

Shiff SJ, Rigas B (1999) The role of cyclooxygenase inhibition in the antineoplastic effects of nonsteroidal antiinflammatory drugs (NSAIDs). *J Exp Med* **190:** 445–450

Srinivasan S, Sadegh L, Elle IC, Christensen AG, Faergeman NJ, Ashrafi K (2008) Serotonin regulates C. elegans fat and feeding through independent molecular mechanisms. *Cell Metab* **7:** 533–544

Steinmetz AC, Renaud JP, Moras D (2001) Binding of ligands and activation of transcription by nuclear receptors. *Annu Rev Biophys Biomol Struct* **30:** 329–359

Tontonoz P, Hu E, Spiegelman BM (1994) Stimulation of adipogenesis in fibroblasts by PPARγ2, a lipid-activated transcription factor. *Cell* **79:** 1147–1156

Vindis C, Séguélas MH, Lanier S, Parini A, Cambon C (2001) Dopamine induces ERK activation in renal epithelial cells through H₂O₂ produced by monoamine oxidase. *Kidney Int* **59:** 76–86

Waki H, Park KW, Mitro N, Pei L, Damoiseaux R, Wilpitz DC, Reue K, Saez E, Tontonoz P (2007) The small molecule harmine is an antidiabetic cell-type-specific regulator of PPARγ expression. *Cell Metab* **5:** 357–370

Waku T, Shiraki T, Oyama T, Fujimoto Y, Maebara K, Kamiya N, Jingami H, Morikawa K (2009a) Structural insight into PPARγ activation through covalent modification with endogenous fatty acids. *J Mol Biol* **385:** 188–199

Waku T, Shiraki T, Oyama T, Morikawa K (2009b) Atomic structure of mutant PPARγ LBD complexed with 15d-PGJ$_2$: novel modulation mechanism of PPARγ/RXRα function by covalently bound ligands. *FEBS Lett* **583:** 320–324

Walczak R, Tontonoz P (2002) PPARadigms and PPARadoxes: expanding roles for PPARγ in the control of lipid metabolism. *J Lipid Res* **43:** 177–186

Xu HE, Lambert MH, Montana VG, Plunket KD, Moore LB, Collins JL, Oplinger JA, Kliewer SA, Gampe Jr RT, McKee DD, Moore JT, Willson TM (2001) Structural determinants of ligand binding selectivity between the peroxisome proliferator-activated receptors. *Proc Natl Acad Sci USA* **98:** 13919–13924

Yadav VK, Balaji S, Suresh PS, Liu XS, Lu X, Li Z, Guo XE, Mann JJ, Balapure AK, Gershon MD, Medhamurthy R, Vidal M, Karsenty G, Ducy P (2010) Pharmacological inhibition of gut-derived serotonin synthesis is a potential bone anabolic treatment for osteoporosis. *Nat Med* **16:** 308–312